

**Localized patterns in star networks of class-B lasers with optoelectronic feedback**J. Shena,<sup>1,2</sup> J. Hizanidis,<sup>1,2,\*</sup> N. E. Kouvaris,<sup>3</sup> and G. P. Tsironis<sup>1,2</sup><sup>1</sup>*Department of Physics, University of Crete, 71003 Heraklion, Greece*<sup>2</sup>*National University of Science and Technology MISis, Leninsky Prospect 4, Moscow, 119049, Russia*<sup>3</sup>*Department of Mathematics, Namur Institute for Complex Systems (naXys), University of Namur, Rempart de la Vierge 8, B 5000 Namur, Belgium*

(Received 9 July 2018; published 12 November 2018)

We analyze how a star network topology shapes the dynamics of coupled CO<sub>2</sub> lasers with an intracavity electro-optic modulator that exhibits bistability. Such a network supports spreading and stationary activation patterns. In particular, we observe an activation spreading where the activated periphery turns on the center element, an activated center which drifts the periphery into the active region, and an activation of the whole system from the passive into the active region. Pinned activation, namely activation localized only in the center or the peripheral elements, is also found. Similar dynamical behavior has been observed recently in complex networks of coupled bistable chemical reactions. The current work aims at revealing those phenomena in laser arrays, giving emphasis to the essential role of the coupling structure in fashioning the overall dynamics.

DOI: [10.1103/PhysRevA.98.053817](https://doi.org/10.1103/PhysRevA.98.053817)**I. INTRODUCTION**

Solid-state, gas, and semiconductor laser arrays constitute a wide family of nonlinear coupled systems with complex dynamic behavior. Although the total light emission from these arrays may be stable, the emission from individual elements of an array is often unstable with large amplitude chaotic pulsations [1–3]. Moreover, the coupled system can show synchronization and other spatiotemporal phenomena [4]. The main difference between conventional semiconductor and solid-state or gas lasing media lies in the value of the linewidth enhancement factor  $a$ , which is  $2 \leq a \leq 5$  for semiconductor lasers and  $a = 0$  for solid-state or gas systems [5]. This difference makes solid-state or gas lasers more suitable in applications where phase locking is required, which is the case in our current study. Another important difference lies in the effect of the delay time, which in the case of coupled solid-state or gas lasers can be neglected, while in coupled semiconductor lasers it may lead to the appearance of multiple locked states [6]. In our analysis we neglect the dynamics of the phase differences between the electric fields, so by choosing gas lasers we achieve a range of parameters for phase locking wider than that for semiconductor lasers.

In recent years, there have been many studies concerning semiconductor laser arrays and the analysis of synchronization and chimera states [7–10]. Another rapidly growing field with significant technological applications that involves networks of lasers is the field of neuromorphic photonics [11,12]: When a laser is in the excitable regime it exhibits spiking dynamics similar to a biological neuron, but approximately 8 orders of magnitude faster. An integrated network on a chip of such “laser neurons” could provide a wide range of significant computing and signal-processing applications. In the present

work, we focus on gas laser arrays and the formation of localized stationary patterns of activity. The dynamic behavior of each laser element is bistable and the coupling between the elements is local and arises due to the overlap of the electric fields of each separated beam [2,13]. The theoretical model we use is originated from numerical and experimental studies of a CO<sub>2</sub> laser with an intracavity electro-optic modulator that exhibits bistability [14]. The repeated reference to solid-state lasers is done because a similar problem was revisited for a Nd:YAG laser with an acousto-optic modulator [15]. However, our model has many similarities to that obtained by semiconductor lasers with a saturable absorber inside the cavity [16]. Moreover, bistability was also found in semiconductor lasers with strong optical injection [17] and in semiconductor laser diodes with a saturable absorber [18].

Other classical examples where bistable behavior is encountered are dynamical processes in chemical systems [19,20]. Recently, studies on complex networks of coupled bistable chemical reactions revealed rich collective dynamics, such as spreading or retreating of an initial activation, but more interestingly, the formation of localized stationary patterns dependent on the coupling strength and the degree distribution of the nodes [21–24]. Beyond the simplified theoretical approach, electrochemical experiments [23,24] have stressed that the coupling topology plays a significant role in the observed dynamics resulting in a robust pattern formation mechanism. Therefore, similar findings are expected to be seen in laser arrays coupled in such a way, thus forming complex networks.

Here we focus on the simple case of star networks where each bistable element is connected to a central one, the hub. This connectivity structure is often found in many natural or engineered systems that consist of dynamical elements interacting with each other through a common medium. It has also been used in optically coupled semiconductor lasers [25,26] where synchronization phenomena were investigated. We

\*hizanidis@physics.uoc.gr

present an extended numerical analysis that takes advantage of the simplicity of the star network topology to determine the conditions required for the formation of localized stationary patterns. We start our investigation by analyzing the dynamics and determining the bistable regime for a single laser. In the bistable regime the active and the passive states of the laser coexist. Knowing this we explore the dynamics of two coupled bistable lasers, before we proceed to our main study for a star network of such elements. This work comments on the formation mechanism of stationary patterns which—like in the electrochemical networks—is strongly dependent on the role of the coupling topology.

## II. THE MODEL

The dynamical behavior of the CO<sub>2</sub> laser with feedback can be described by three coupled first-order differential equations, one for the laser field ( $E$ ), the second for the population inversion ( $G$ ), and the last for the feedback voltage of the electro-optic modulator ( $V$ ). In dimensionless form, the evolution equations have the following form [14]:

$$\frac{dE}{dt} = \frac{1}{2}[G - 1 - a \sin^2(V)]E, \quad (1a)$$

$$\frac{dG}{dt} = \gamma(P - G - G|E|^2), \quad (1b)$$

$$\frac{dV}{dt} = \beta(B + f|E|^2 - V), \quad (1c)$$

where  $|E|$  is the amplitude of electric field,  $\gamma$  denotes the population decay time,  $P$  denotes the pumping, and  $a$  scales the maximum loss introduced by the modulator. The damping rate  $\beta$  of the feedback loop is normalized to the cavity decay rate,  $B$  is the bias voltage applied to the modulator amplifier, and  $f$  is the scaling of the feedback gain, i.e., it measures the relation between the intensity incident on the photodiode and the voltage delivered by the differential amplifier. In general,  $B$  is used as a control parameter.

In the case of a single laser, the phase of the electric field is a constant variable in time and has no role in the system dynamics [27]. Thus, we prefer to work with the amplitude of the electric field without loss of generality. In this framework, the system of Eqs. (1) admits the zero-intensity solution ( $|E| = 0$ ,  $G = P$ ,  $V = B$ ) and the nonzero intensity solution, which are given in the following parametric form:

$$\frac{P}{1 + |E|^2} = 1 + a \sin^2(B + f|E|^2), \quad (2a)$$

$$G = \frac{P}{1 + |E|^2},$$

$$V = B + f|E|^2. \quad (2b)$$

Figure 1 illustrates the stability of these fixed points by studying the bifurcation diagram in the case of high gain  $f = -0.6$  and using  $B$  as the control parameter [14].

For  $B < 0.3441$ , the zero-intensity fixed point is unstable (marked by the dashed line), and the nonzero-intensity solution is the only attractor in the system (active state). At  $B = 0.3441$ , a subcritical pitchfork bifurcation (PB) takes place and the zero-intensity fixed point becomes stable. At the

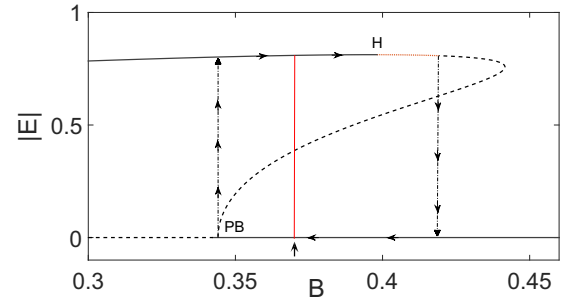


FIG. 1. High-gain bifurcation diagram. The stationary amplitude of the laser field  $|E|$  is shown as a function of the bias voltage  $B$ . The solid and dashed lines mark the stable and unstable branches, respectively, while the arrows indicate the hysteresis loop. H denotes the Hopf bifurcation point and PB the subcritical pitchfork bifurcation. The constant value of  $B = 0.37$  that is used in the following sections has been indicated by the arrow and the red (gray) line. Other parameters are  $\gamma = 0.003125$ ,  $P = 1.66$ ,  $\beta = 0.0521$ ,  $a = 5.8$ , and  $f = -0.6$ . The dotted line denotes a very small regime of low-amplitude oscillations.

same time, a new unstable fixed point is born which vanishes for  $B = 0.3982$ . In the interval  $0.3441 < B < 0.4191$  the system exhibits bistability and a hysteresis loop is observed. As  $B$  increases beyond the value  $0.4191$ , the zero intensity solution is the only allowed state in the system. In the rest of our analysis we hold the bias voltage constant and equal to  $B = 0.37$  in order to achieve a controllable bistable system that can be prepared either in the passive state  $0 < |E| < 0.2$  or the active one  $0.7 < |E| < 0.9$ . Moreover, the chosen value  $B = 0.37$  allows us to avoid transitions from the Hopf point at  $B = 0.3982$ , above which a very small regime of low-amplitude oscillations exists (marked by the dotted line). The bifurcation diagrams throughout the manuscript have been generated using the MATCONT software, a numerical continuation package for the interactive bifurcation analysis of dynamical systems [28].

## III. TWO COUPLED BISTABLE LASERS

Having defined the single bistable laser system, we proceed by considering two parallel waveguides of CO<sub>2</sub> lasers, each one with a proper optoelectronic feedback (see Fig. 2). The mutual interaction lies on the overlap integrals of both lasers fields inside the crystal with a proper refractive index profile [13]. The evolution equations for this coupled system have the following form:

$$\frac{dE}{dt} = \frac{E}{2}[G - 1 - a \sin^2(V)] + \eta E_H, \quad (3a)$$

$$\frac{dE_H}{dt} = \frac{E_H}{2}[G_H - 1 - a \sin^2(V_H)] + \eta E, \quad (3b)$$

where the subscript H denotes the second laser. The equations for the population inversion ( $G$  and  $G_H$ ) and the feedback voltage of the modulator ( $V$  and  $V_H$ ) have the same form as in Eqs. (1); therefore we omit them. The parameter  $\eta$  is the coupling strength between the two lasers and in general is a complex parameter ( $\eta = \eta_{\text{Re}} + i\eta_{\text{Im}}$ ). The real part  $\eta_{\text{Re}}$  takes

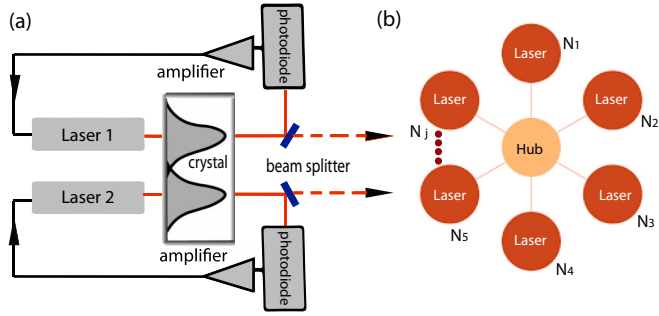


FIG. 2. (a) Schematic diagram of the optoelectronic feedback of two coupled lasers. The optical power emitted by the two lasers is coupled through the overlap of the electrical fields in a nonlinear crystal. After a beam splitter, it is detected by a photodiode with a fixed bandwidth. The electrical output is fed back to each laser through an amplifier. (b) Topology of a star network where each laser of the periphery interacts with the rest through a central laser, the hub, with the same coupling strength.

usually negative values and vanishes only when  $D \simeq 2w$ , where  $D$  is the distance between the two beams and  $w$  is the waist of the beam Gaussian portrait. However, it is possible to have positive coupling values, which we consider here, by pumping in the middle between the two beams [29]. The imaginary part  $\eta_{\text{Im}}$  is related to the refractive index and can be zero for a laser beam of weak intensity, which is the case here. If we use the polar coordinates  $E = |E|e^{i\phi}$ , a third equation for the phase difference of the two lasers is added to Eqs. (3). However, we can neglect the dynamics of the third variable since we are working in the phase-locking regime, i.e., the phase difference is constant and equal to zero (see Fig. 5 in Appendix A). The dynamics of the system can, therefore, be described solely by the amplitude of the electric field.

The zero-intensity steady state of the coupled system is equal to  $|E| = |E_H| = 0$ ,  $G = G_H = P$ , and  $V = V_H = B$ , while the nonzero-intensity steady states of Eqs. (3), are given in the following parametric form:

$$\frac{P}{1 + |E|^2} = 1 + a \sin^2(B + f|E|^2) + 2\eta \frac{|E_H|}{|E|}, \quad (4a)$$

$$\frac{P}{1 + |E_H|^2} = 1 + a \sin^2(B + f|E_H|^2) + 2\eta \frac{|E|}{|E_H|}. \quad (4b)$$

Figure 3 shows the stability of the system steady states as a function of the coupling strength. Figure 3(a) shows the stationary amplitude of the electric fields in the case where the system is prepared with the first laser in the passive state and the second one in the active state. Similarly, Fig. 3(b) shows the stability of the system when both lasers are prepared in the active state. In Fig. 3(c) the two previous cases (passive-active, active-active) are plotted together with the passive-passive state which corresponds to the black dash-dotted line. Figure 3(d) shows the stability region for the amplitude of both lasers in all three cases is shown in the  $(|E|, |E_H|)$  plane, with the passive-passive state represented by a solid black circle. The dashed lines correspond to the unstable solution branches. From Fig. 3(c) we can see that the passive-passive

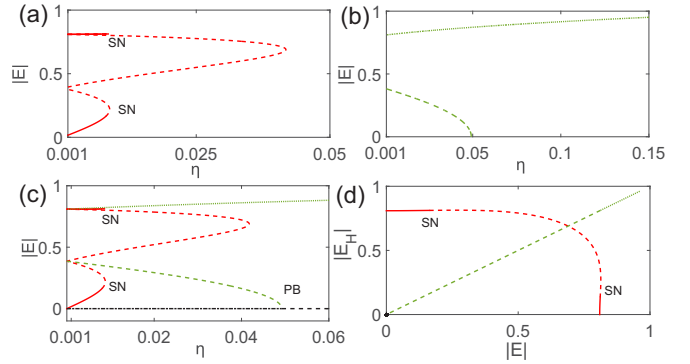


FIG. 3. The stationary amplitude of the laser field versus the coupling strength. (a) The amplitude of the first laser in the case where the system is prepared with the first laser located in the passive state and the second in the active state (passive-active). (b) The stationary amplitude of the laser field versus the coupling strength where both the two lasers are located in the active state (active-active). (c) The stability for all three preparation states of the system (passive-active, active-active and passive-passive). (d) The stability region for the amplitude of both lasers in all three cases is shown in the  $(|E|, |E_H|)$  plane. Solid, dotted and dash-dotted lines correspond to stable states while dashed lines correspond to unstable steady states. SN stands for the saddle-node bifurcation, while PB for the subcritical pitchfork.  $B = 0.37$  and all other parameters as in Fig. 1.

state (black dash-dotted line) undergoes a subcritical PB at  $\eta = 0.04922$ . The passive-active state [red (gray) line] is stable up to a critical coupling strength of  $\eta = 0.008819$ , where a saddle-node bifurcation (SN) occurs, and the active-active state (green dotted line) is stable for the whole  $\eta$  range and coexists with an unstable branch that emerges at the PB point and runs through the negative axis (not shown here because  $\eta$  has physical meaning only for positive values).

As a result of the above stability analysis, when the system starts at the passive-active state, both lasers jump to the active state [green (dotted) line] through a SN bifurcation at rather low coupling strengths of  $\eta > 0.008819$ . This resembles the chemical bistable media where an activation front can propagate, thus activating the passive nodes [23,24]. On the other hand, when the system is prepared in the passive-passive state, higher values of  $\eta > 0.04922$  are required for the lasers to jump to the active-active state, and this transition takes place through a PB bifurcation. This spontaneous activation arises for the actual nature of the coupled laser system and is not observed in chemical bistable media [23,24]. Finally, if the system is prepared in the active-active state (green dotted line), both lasers will remain there for all values of the coupling strength.

#### IV. STAR NETWORK OF COUPLED BISTABLE LASERS

Having analyzed the dynamics of two coupled bistable lasers, we now focus on a star network configuration and how it contributes to the formation mechanism of stationary active patterns. In such a system each element of the periphery

interacts with the rest through a central element, the hub [see Fig. 2(b)], and thus Eqs. (3) can be reformulated as follows:

$$\frac{dE_j}{dt} = \frac{E_j}{2}[G_j - 1 - a \sin^2(V_j)] + \eta E_H, \quad (5a)$$

$$\frac{dE_H}{dt} = \frac{E_H}{2}[G_H - 1 - a \sin^2(V_H)] + \eta \sum_{j=1}^N E_j, \quad (5b)$$

where  $j = 1, 2 \dots N$  counts for the number  $N$  of the peripheral elements and the subscript  $H$  denotes the hub. In polar coordinates, Eqs. (5) become

$$\frac{d|E_j|}{dt} = \frac{1}{2}|E_j|[G_j - 1 - a \sin^2(V_j)] + \eta|E_H| \cos(\theta_j), \quad (6a)$$

$$\frac{d|E_H|}{dt} = \frac{1}{2}|E_H|[G_H - 1 - a \sin^2(V_H)] + \eta \sum_{j=1}^N |E_j| \cos(\theta_j), \quad (6b)$$

$$\frac{d\theta_j}{dt} = -\eta \left[ \frac{|E_H|}{|E_j|} \sin(\theta_j) + \sum_{k=1}^N \frac{|E_k|}{|E_H|} \sin(\theta_k) \right], \quad (6c)$$

where  $\theta_j = \phi_H - \phi_j$  are the phase differences between the electric fields of each node of the periphery and that of the hub. The equations for the variables  $G_j$ ,  $V_j$ ,  $G_H$ , and  $V_H$  have the same form as Eqs. (1) and, again, we omit them. Numerical integration of Eqs. (6) shows that in the  $N$ - $\eta$  parameter space the phase differences  $\theta_j$  remain constant and equal to zero for  $\eta > 0.002$  (see Fig. 6 in Appendix A). Therefore, Eq. (6c) can be neglected, the cosine terms are equal to 1, and the index  $j$  can be dropped, reducing the star network to a system of two coupled lasers with asymmetric coupling:

$$\frac{d|E|}{dt} = \frac{1}{2}|E|[D - 1 - a \sin^2(V)] + \eta|E_H|, \quad (7a)$$

$$\frac{d|E_H|}{dt} = \frac{1}{2}|E_H|[D_H - 1 - a \sin^2(V_H)] + \eta N|E|. \quad (7b)$$

Previous studies with electrochemical systems [23,24,30] have implemented similar methods for reducing star and tree networks to chains of asymmetrically coupled nodes. In those theoretical and experimental studies, it was demonstrated that such a reduced system could produce all the rich dynamics of the original network despite its simpler form.

Again, the zero-intensity solution corresponds to  $|E| = |E_H| = 0$ ,  $G = G_H = P$ , and  $V = V_H = B$ , and the nonzero-intensity solutions are given in the following parametric form:

$$\frac{P}{1 + |E|^2} - 1 - a \sin^2(B + f|E|^2) = -2\eta \frac{|E_H|}{|E|}, \quad (8a)$$

$$\frac{P}{1 + |E_H|^2} - 1 - a \sin^2(B + f\varepsilon_H^2) = -2\eta N \frac{|E|}{|E_H|}. \quad (8b)$$

In the previous section, the system of two symmetrically coupled lasers has shown that, depending on the preparation of the coupled system, the lasers' transition to the active state occurs through either a saddle-node bifurcation or a

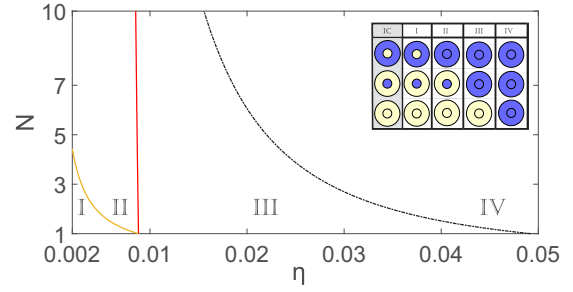


FIG. 4. Phase diagram in the  $(\eta, N)$  parametric space. Four dynamical regions are separated by lines that correspond to the continuation of the bifurcation points shown in Fig. 3. Orange (gray) and red (dark gray) lines correspond to saddle-node bifurcation lines, while the black line corresponds to a pitchfork bifurcation line. In region I the coupling is weak enough and all three initial conditions (IC) shown in the inset are stable and consist steady states of the system. In region II the active periphery drifts the hub to the active state. In region III the active periphery drifts the hub to the active state but also the active hub drifts to the periphery in the active state. In region IV the whole network goes to the active state. In the inset the inner circle represents the hub and the outer circle represents the periphery, while the active state is denoted with blue (dark gray) and the passive state with yellow (light gray). Other parameters are as in Fig. 3.

subcritical pitchfork bifurcation. In order to locate these transitions in the star network, we perform a continuation of the bifurcations in the  $(\eta, N)$  parameter space as shown in Fig. 4. The orange (gray) line separating regions I and II corresponds to the continuation of the SN bifurcation in the case where the hub starts in the passive state and the periphery in the active state. Our reduced system with the two asymmetrically coupled lasers is directed; therefore the passive-active state stability should be considered for the opposite case as well, i.e., for the hub in the active state and the periphery in the passive state. This latter red (dark gray) bifurcation line starts at the same coupling strength value as the previous bifurcation line, but has a different behavior and separates the regions II and III. Finally, the black line separating regions III and IV corresponds to the continuation of the PB bifurcation that marks the transition from the passive-passive state to the active-active state. Note that all three lines are continuous for the sake of representation. The physically valid points correspond to  $N$  values equal to natural numbers.

These bifurcation lines separate the  $(\eta, N)$  parameter space into four distinct regions where the system reaches different steady states. In region I, any initial condition (periphery active–hub passive, periphery passive–hub active, or periphery passive–hub passive) remains as it is; i.e., the system is pinned to its initial preparation. In region II, the active periphery drifts the passive hub into the active state. The same occurs in region III where, additionally, the active hub drifts the passive periphery into the active state. In this region the activation propagates faster from the active periphery towards the passive hub than from an active hub towards the periphery. Finally, in region IV the coupling strength is strong enough even for the periphery passive–hub passive initial condition to jump to the active-active state. An example of the described

dynamical behaviors is shown in the inset of Fig. 4, where the evolution of three initial conditions (IC) in the  $(\eta, N)$  parameter space is illustrated. The outer circle represents the periphery of the system and the inner circle represents the hub, while light and dark colors correspond to the passive and active states, respectively.

In close analogy to previous findings in electrochemical bistable networks [23,24], Fig. 4 shows that the coupling strength required for a transition to occur in the system's dynamics depends on the number of peripheral nodes. The orange (gray) line separating regions I and II drops with  $\eta$  because, as the coupling strength increases, a smaller  $N$  size is needed for the periphery to activate the hub (and vice versa). This results in a shift to lower  $\eta$  values of the position of the saddle-node bifurcation when  $N$  increases [see Fig. 7(b) in Appendix B]. On the other hand, the number of periphery nodes is almost [red (dark gray) line has a tiny slope] independent of the coupling strength required for the hub to activate the periphery [red (dark gray) line, and see Fig. 7(c) of Appendix B]. Finally, the black line separating regions III and IV, which marks the activation of both passive hub and passive periphery, exists for higher values of the coupling strength and, similarly to the orange (gray) line, drops with  $\eta$  [see Fig. 7(d) of Appendix B].

## V. CONCLUSIONS

We have shown that star networks of coupled bistable class-B lasers support activation spreading from the hub towards the peripheral elements and vice versa. Interestingly, stationary patterns of activation localized on the hub or the peripheral nodes are also supported, determined by the number of coupled lasers to the central unit, by the coupling strength, and by the initial conditions. Similar findings were previously reported for electrochemical systems. However, the system considered in the current work has been implemented for coupled CO<sub>2</sub> lasers with optoelectronic feedback keeping the bias voltage applied to the modulator constant and by considering the coupling strength as a control parameter. Extensive numerical calculations show that the phases of the central laser and any peripheral unit lock after a very small time interval, allowing us to investigate only the steady state of the system.

In a system size–coupling strength diagram we demonstrate four distinct regions indicating different dynamical behavior. At weak coupling strengths and small network sizes the initial preparation of the system is pinned and an activation remains stationary and localized either on the peripheral elements or on the hub. At weak coupling strengths but larger network sizes an activation can spread only from the periphery towards the hub, but not in the opposite direction. Namely, an activated periphery turns on the center element, but an activated hub cannot drift the periphery to the active state. This occurs for moderate values of the coupling strength. In this third region, activation spreads in both directions (with different velocities) and an activated periphery turns on the hub and an activated hub can drift the periphery into the active state. Finally, an activation of the whole system from the passive state into the operative region (active state) is shown for strong couplings.

Despite the obviously different nature of the considered system from that of the previously studied electrochemical networks, our findings have essential similarities, indicating that the network connectivity affects the hosted bistable dynamics in an akin fashion. The ability to control the spreading or the pinning of an activation, and thus the dynamics of the system from the passive state into the active state and vice versa, may have multiple technological applications especially in neuromorphic photonics [11,12], where such treelike networks can serve as simple hierarchical connectivity structures. For future studies, it would be worthwhile to explore if those stationary states can live in the presence of small phase perturbations, due to spontaneous emission or through the detuning of each individual laser cavity length. Moreover, it would be interesting to consider the bias regime where the system exhibits oscillations, and instead of the CO<sub>2</sub> laser, it would be interesting to study a semiconductor laser diode with a saturable absorber.

## ACKNOWLEDGMENTS

This work was supported by the Ministry of Education and Science of the Russian Federation in the framework of the Increase Competitiveness Program of NUST “MISiS” (Grant No. K2-2017-006). N.E.K acknowledges financial support by the “MOVE-IN Louvain” Fellowship, cofunded by the Marie Curie Actions of the European Commission. This research has been financially supported by the General Secretariat for Research and Technology (GSRT) and the Hellenic Foundation for Research and Innovation (HFRI) (Code: 203).

## APPENDIX A: PHASE-LOCKING REGIME

By numerically integrating Eqs. (6) for 100 different initial conditions of the phase differences  $\theta_j$  in the interval  $[-\pi, \pi]$ , we have calculated the mean value  $\theta$  in the  $\eta$ - $t$  parameter space. The time is in units of the relaxation period  $T_R = 2\pi/\omega_R$ , where  $\omega_R = \sqrt{k\gamma_{\parallel}}$ . Typical values for the cavity loss and the population decay in a CO<sub>2</sub> laser are  $k = 9.6 \times 10^6 \text{ s}^{-1}$  and  $\gamma_{\parallel} = 3 \times 10^4 \text{ s}^{-1}$ , respectively. The integration has been done using a fourth-order Runge-Kutta algorithm with a fixed time step ( $dt = 0.0001T_R$ ). In Fig. 5 we can see that after a time period equal to  $100T_R$  and for  $\eta > 0.001$  the mean phase difference  $\langle \theta \rangle$  goes to zero. Figure 5(a) corresponds to a system prepared in either the passive-passive state or the active-active state, while Fig. 5(b) refers to the active-passive (passive-active) initialization state.

In order to investigate the phase-locking regime for  $\eta > 0.002$  in the whole  $N$ - $\eta$  parameter space, we calculate a phase-order parameter which is defined as follows [31]:

$$\Delta_q = \left\langle \frac{1}{N} \left| \sum_{j=1}^N e^{\theta_j - (j-1)q} \right| \right\rangle, \quad (\text{A1})$$

which is unity for the fully ordered system and zero when the system is completely disordered. Here,  $q$  is the expected phase difference between oscillators and the averaging is done over realizations of different initial conditions for  $\theta_j$  in the interval  $[-\pi, \pi]$ . In our case the phase differences converge to zero; hence the  $q$  parameter is zero. In Fig. 6

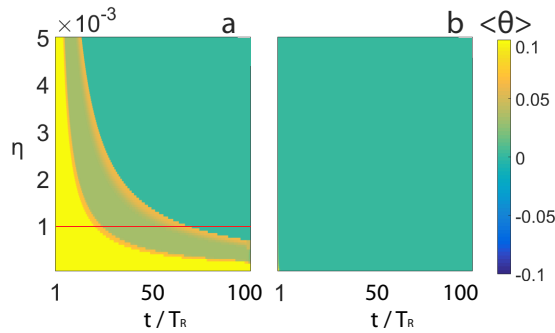


FIG. 5. The mean value of  $\theta$  in the  $\eta$ - $t$  space over 100 different initial conditions of the phase difference in the interval  $[-\pi, \pi]$ . (a) Initial preparation of the system in the passive-passive state or the active-active state. (b) Initial preparation of the system in the active-passive state or the passive-active state. The red (dark gray) line indicates the constant value of  $\eta = 0.001$ . Other parameters are  $\gamma = 0.003125$ ,  $P = 1.66$ ,  $\beta = 0.0521$ ,  $a = 5.8$ , and  $f = -0.6$ .

we have calculated  $\Delta_0$  in the  $\eta$ - $t$  parameter space for  $N = 3$  and 5 and  $N = 7$  periphery nodes. As we can see, for  $\eta > 0.002$  the phase-order parameter  $\Delta_0 \sim 1$ . This holds for all three initial preparations of the system (periphery passive–hub

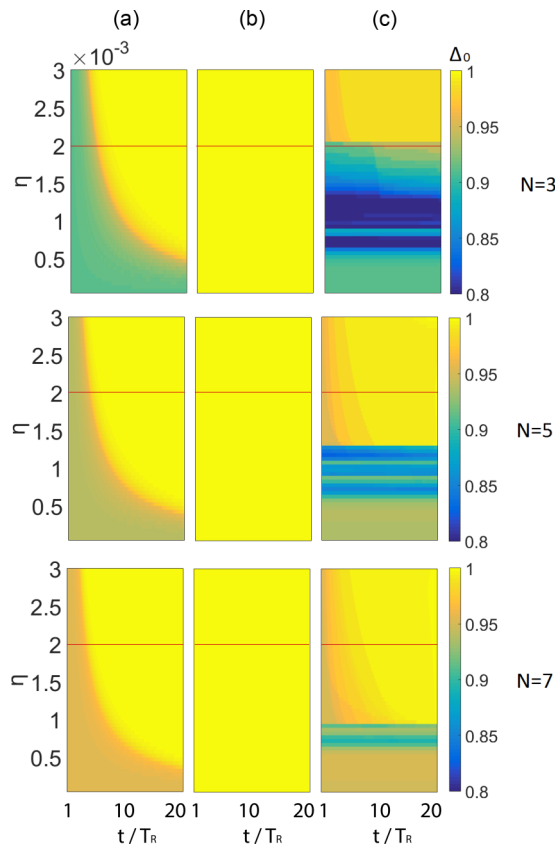


FIG. 6.  $\Delta_0$  in the  $\eta$ - $t$  space for  $N = 3$  (top),  $N = 5$  (middle), and  $N = 7$  (bottom). System initializations are as follows: (a) periphery passive–hub passive, (b) periphery passive–hub active state, and (c) periphery active–hub passive. The red (dark gray) line indicates the constant value of  $\eta = 0.002$ . Other parameters are as in Fig. 5.

passive, periphery passive–hub active, and periphery active–hub passive).

## APPENDIX B: BIFURCATION DIAGRAMS FOR THE LASER STAR NETWORK

In Fig. 7 we have calculated the stationary amplitude of the laser field versus the coupling strength for a star network of varying size. In Figs. 7(a) and 7(c) we plot the stationary amplitude of the periphery laser, while the amplitude of the hub laser is shown in Figs. 7(b) and 7(d). Black (dark gray) corresponds to a star network with three periphery nodes, red (gray) to a star network with five periphery nodes, and blue (light gray) to a star network with seven periphery nodes. The state hub passive–periphery active is shown in Figs. 7(a) and 7(b), while the opposite state (hub active–periphery passive) is shown in Figs. 7(c) and 7(d). The hub passive–periphery passive state and the hub active–periphery active state are plotted in all four panels of Fig. 7.

In Fig. 7(a) we observe that the active stable region remains active for any periphery size, while the passive stable region becomes smaller with increasing periphery size. When the hub is in the passive state and the periphery is in the active state, by increasing the number of peripheral nodes the critical coupling strength for which the hub becomes active decreases [see Fig. 7(b)]. The reason for this behavior is the  $\eta$ - $N$  dependence of the periphery on the hub laser. This does not happen in the opposite case, where the increase of the peripheral nodes has no significant effect on this transition, due to the  $\eta$  dependence of the hub laser on the periphery [see Fig. 7(c)]. Finally, in Fig. 7(a) we see that the active stable region remains active and independent of the periphery size.

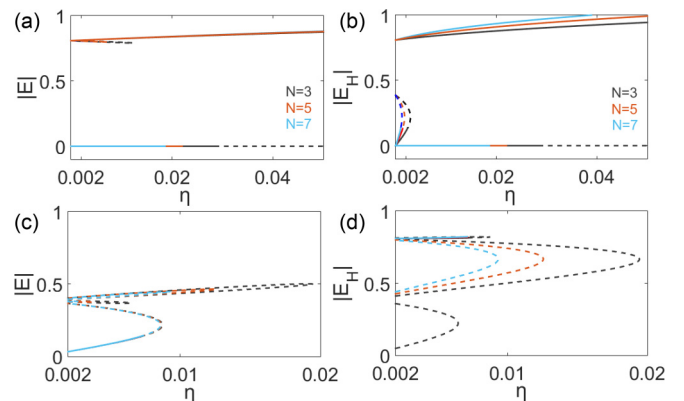


FIG. 7. The stationary amplitude of the laser field versus the coupling strength for a star network with three nodes in the periphery [black (dark gray)], five nodes [red (gray)], and seven nodes [blue (light gray)]. Panels (a) and (c) show the amplitude of the periphery laser, and panels (b) and (d) show the amplitude of the hub laser. The hub passive–periphery passive and the hub active–periphery active states have been plotted in all four panels. The state hub passive–periphery active is shown in panels (a) and (b), while the opposite state (hub active–periphery passive) is shown in panels (c) and (d). Solid and dashed lines correspond to the stable and unstable branches, respectively. Other parameters are as in Fig. 5.

- [1] S. S. Wang and H. G. Winful, *Appl. Phys. Lett.* **52**, 1774 (1988).
- [2] L. Fabiny, P. Colet, R. Roy, and D. Lenstra, *Phys. Rev. A* **47**, 4287 (1993).
- [3] K. S. Thornburg, M. Möller, R. Roy, T. W. Carr, R.-D. Li, and T. Erneux, *Phys. Rev. E* **55**, 3865 (1997).
- [4] F. Rogister and R. Roy, *Phys. Rev. Lett.* **98**, 104101 (2007).
- [5] B. Kelleher, C. Bonatto, G. Huyet, and S. P. Hegarty, *Phys. Rev. E* **83**, 026207 (2011).
- [6] C. Bonatto, B. Kelleher, G. Huyet, and S. P. Hegarty, *Phys. Rev. E* **85**, 026205 (2012).
- [7] H. G. Winful, *Phys. Rev. A* **46**, 6093 (1992).
- [8] F. Böhm, A. Zakharova, E. Schöll, and K. Lüdge, *Phys. Rev. E* **92**, 069905(E) (2015).
- [9] J. Shena, J. Hizanidis, V. Kovanis, and G. P. Tsironis, *Sci. Rep.* **7**, 42116 (2017).
- [10] J. Shena, J. Hizanidis, P. Hövel, and G. P. Tsironis, *Phys. Rev. E* **96**, 032215 (2017).
- [11] P. R. Prucnal, J. B. Shastri, T. Ferreira De Lima, M. A. Nahmias, and A. N. Tait, *Adv. Opt. Photonics* **8**, 228 (2016).
- [12] T. Ferreira De Lima, J. B. Shastri, A. N. Tait, M. A. Nahmias, and P. R. Prucnal, *Nanophotonics* **6**, 577 (2017).
- [13] V. Zehnlé, *Phys. Rev. A* **62**, 033814 (2000).
- [14] P. Ye Wang, A. Lapucci, R. Meucci, and F. T. Arecchi, *Opt. Commun.* **80**, 42 (1990).
- [15] R. Meucci, R. McAllister, and R. Roy, *Phys. Rev. E* **66**, 026216 (2002).
- [16] M. Yamada, *IEEE J. Quantum Electron.* **29**, 1330 (1993).
- [17] S. Wiczorek, T. B. Simpson, B. Krauskopf, and D. Lenstra, *Phys. Rev. E* **65**, 045207 (2002).
- [18] J. L. A. Dubbeldam and B. Krauskopf, *Opt. Commun.* **159**, 325 (1999).
- [19] A. S. Mikhailov, *Foundations of Synergetics I: Distributed Active Systems* (Springer, Berlin, 1990).
- [20] I. R. Epstein and J. A. Pojman, *An Introduction to Nonlinear Chemical Dynamics: Oscillations, Waves, Patterns, and Chaos* (Oxford University, London, 1998).
- [21] N. E. Kouvaris, H. Kori, and A. S. Mikhailov, *PLoS One* **7**, e45029 (2012).
- [22] N. E. Kouvaris and A. S. Mikhailov, *Europhys. Lett.* **102**, 16003 (2013).
- [23] N. E. Kouvaris, M. Sebek, A. S. Mikhailov, and I. Z. Kiss, *Angew. Chem., Int. Ed.* **55**, 13267 (2016).
- [24] N. E. Kouvaris, M. Sebek, A. Iribarne, A. Díaz-Guilera, and I. Z. Kiss, *Phys. Rev. E* **95**, 042203 (2017).
- [25] J. Zamora-Munt, C. Masoller, J. Garcia-Ojalvo, and R. Roy, *Phys. Rev. Lett.* **105**, 264101 (2010).
- [26] M. Bourmpos, A. Argyris, and D. Syvridis, *J. Lightwave Technol.* **30**, 2618 (2012).
- [27] T. Erneux and P. Glorieux, *Laser Dynamics* (Cambridge University, Cambridge, England, 2010).
- [28] W. Govaerts, Y. A. Kuznetsov, V. De Witte, A. Dhooge, H. Meijer, W. Mestrom, A. Riet, and B. Sautois, *MATCONT and CL MATCONT: Continuation toolboxes in MATLAB*, 2011.
- [29] H. Laabs and B. Ozygus, *Opt. Laser Technol.* **29**, 401 (1997).
- [30] M. Wickramasinghe, E. M. Mrugacz, and I. Z. Kiss, *Phys. Chem. Chem. Phys.* **13**, 15483 (2011).
- [31] M. Giver, Z. Jabeen, and B. Chakraborty, *Phys. Rev. E* **83**, 046206 (2011).